

Development of DynamicMC for PHITS Monte Carlo package

Hiroshi Watabe¹, Tatsuhiko Sato², Kwan Ngok Yu³, Milena Zivkovic⁴, Dragana Krstic⁴, Dragoslav Nikezic^{4,5}, Kyeong Min Kim⁶, Taiga Yamaya⁷, Naoki Kawachi⁸, Hiroki Tanaka⁹, A.K.F. Haque¹⁰, M. Rafiqul Islam¹¹ and Mehrdad Shahmohammadi Beni^{1,3,*}

¹Division of Radiation Protection and Safety Control, Cyclotron and Radioisotope Center, Tohoku University, 6-3 Aoba, Aramaki, Aoba-ku, Sendai, Miyagi 980-8578, Japan

²Nuclear Science and Engineering Center, Japan Atomic Energy Agency, 2-4 Shirakata, Tokai, Ibaraki 319-1195, Japan

³Department of Physics, City University of Hong Kong, Tat Chee Avenue, Kowloon Tong, Hong Kong, China

⁴Faculty of Science, University of Kragujevac, R. Domanovica 12, 34000 Kragujevac, Serbia

⁵Department of Natural Sciences and Mathematics, State University of Novi Pazar, Vuka Karadzica 9, 36300 Novi Pazar, Serbia

⁶Korea Institute of Radiological & Medical Sciences, 75, Nowon-ro, Nowon-gu, Seoul 139-706, Korea

⁷National Institutes for Quantum Science and Technology, Anagawa 4-9-1, Inage-ku, Chiba-shi, Chiba 263-8555, Japan

⁸National Institutes for Quantum Science and Technology, 1233 Watanuki, Takasaki, Gunma 370 1292, Japan

⁹Institute for Integrated Radiation and Nuclear Science, Kyoto University, 2-1010 Asashiro-Nishi, Kumatori-cho, Sennan-gun, Osaka 590-0494, Japan

¹⁰Atomic and Molecular Physics Laboratory, Department of Physics, University of Rajshahi, Rajshahi 6205, Bangladesh

¹¹Institute of Nuclear Medical Physics, AERE, Bangladesh Atomic Energy Commission, Dhaka 1349, Bangladesh

*Corresponding author: mehrdad.shahmohammadi.beni.d5@tohoku.ac.jp

Abstract

Previously, we have developed DynamicMC for modeling relative movement of Oak Ridge National Laboratory phantom in a radiation field for the Monte Carlo N-Particle package (Health Physics. 2023,124(4):301–309). Using this software, three-dimensional dose distributions in a phantom irradiated by a certain mono-energetic (Mono E) source can be deduced through its graphical user interface. In this study, we extended DynamicMC to be used in combination with the Particle and Heavy Ion Transport code System (PHITS) by providing it with a higher flexibility for dynamic movement for an anthropomorphic phantom. For this purpose, we implemented four new functions into the software, which are (1) to generate not only Mono E sources but also those having an energy spectrum of an arbitrary radioisotope (2) to calculate the absorbed doses for several radiologically important organs (3) to automatically average the calculated absorbed doses along the path of the phantom and (4) to generate user-defined slab shielding materials. The first and third items utilize the PHITS-specific modalities named radioisotope-source and sumtally functions, respectively. The computational cost and complexity can be dramatically reduced with these features. We anticipate that the present work and the developed open-source tools will be in the interest of nuclear radiation physics community for research and teaching purposes.

Introduction

Ionizing radiations can have detrimental effects on the health of human and living organisms^(1–5); these are due to the energy deposition and subsequent damages that could be induced as a result of interaction of ionising radiations. Considering this, radiation dosimetry is an important yet tedious task when dealing with organs in the human body. In a recent study, Aghaz *et al.*⁽⁶⁾, performed an extensive study

regarding patient-specific dose assessment using Cone-Beam Computed Tomography images and Monte Carlo computations; this highlighted an important methodology in the use of Monte Carlo method to perform patient-specific dose calculation using DICOM images, which, in turn, provided valuable insights for our study. It needs to be noted that several factors can impact the dose deposition in different organs, one being the variation in the distance

Received: June 26, 2023. Revised: October 12, 2023. Editorial decision: October 13, 2023. Accepted: October 16, 2023

© The Author(s) 2023. Published by Oxford University Press. All rights reserved. For Permissions, please email: journals.permissions@oup.com

between the radioactive source and the target⁽⁷⁾. Previously, we have developed a computational model named DynamicMC for modeling relative dynamic movements of a radioactive source with respect to the Oak Ridge National Laboratory (ORNL) human phantom⁽⁸⁾. The developed platform enabled users to model multiple irradiation scenarios and perform organ-based dosimetry by coupling the generated script with Monte Carlo N-Particle (MCNP) package⁽⁹⁾. Furthermore, Phantom with Moving Arms and Legs (PIMAL) program was developed that enabled the users to adjust the posture of a phantom through a user-friendly graphical user interface (GUI)^(10,11); this program was coupled with MCNP Monte Carlo (MC) package. To the best of our knowledge, there are no programs with user-friendly interface for dynamic movement of phantoms that have extensive number features when compared to Particle and Heavy Ion Transport code System (PHITS) DynamicMC.

It was pointed out that the relative movements between the radiation source and exposed targets are important mainly for occupational workers that are moving in radiation fields. These occupational workers include workers in nuclear reactors⁽¹²⁾, medical and radiation workers handling radioactive sources⁽¹³⁾, workers dealing with radioactive wastes^(14,15) and those working in medical imaging facilities such as positron emission tomography⁽¹⁶⁾. The dose monitoring of occupational workers is mostly accomplished using passive detectors usually mounted on their chest. These passive detectors are mostly thermoluminescent dosimeters^(17,18) or glass dosimeters⁽¹⁹⁾ that record the absorbed radiation dose. The issues with these passive detectors include (1) the types of ionising radiation (either primary or secondary radiation) will not be differentiated and (2) the specific absorbed dose in each organ in the human body will not be determined. In order to tackle these issues, the MC method in combination with human phantom models would make it possible to determine the absorbed doses from different types of ionising radiations in different organs^(20,21), hence enabling organ-based dosimetry.

The initial version of the DynamicMC was found to be promising in tackling the issues outlined above, however a few drawbacks would still need to be addressed, namely (1) the models were complex and computationally expensive, (2) only relative movements of the source with respect to the modeled phantom was considered, (3) the initial version only supported coupling with the MCNP package to which some users might not have access and (4) the platform was only developed for GNU/Linux operating systems. For continuous development, it would be pertinent for DynamicMC to be further developed to support different user demands and to address some of the practical drawbacks.

Therefore, in present work we have developed a new version of DynamicMC platform with PHITS MC package support.

The new features that were implemented into the new version of the software are the (1) generation of mono-energetic (Mono E) and source with energy spectrum of an arbitrary radioisotope, (2) absorbed dose computation for several radiologically important organs, (3) automatic averaging of the calculated absorbed doses along the path of the phantom for each source condition and (4) generation of user-defined slab shielding materials. It needs to be noted that item 1 and 3 utilise the PHITS-specific modalities named radioisotope (RI)-source and sumtally functions, respectively. The present version of the DynamicMC provides a higher flexibility of dynamic movement for an anthropomorphic phantom with or without the presence of shielding materials, which, in turn, reduces the computational complexity. In addition, the present model provides the ability to model radioisotope sources with exact energy spectra and decay scheme which would be particularly useful for radiation protection and dosimetry studies. All kinds of radiation from decays (i.e. alpha, beta, gamma-rays and fission neutrons) could be considered using the present program by setting the projectile option to 'all' or any other specific particles. The DECDC⁽²²⁾ nuclear decay database (equivalent to ICRP107) is used to obtain the energy spectra. We strongly believe that the new version of DynamicMC would be a useful tool in the field of nuclear radiation physics and dosimetry. The present computer program and its source code are distributed under GPLv3 license, and users can freely download, modify and redistribute the program without any restrictions.

Materials and methods

Program structure

The present program has seven main parts, namely (1) GUI, (2) graphical coordinate input, (3) dynamic phantom generator, (4) simple script/code viewer, (5) a simple collision detection module, (6) shielding and (7) sumtally generator option. In addition, the present version of the program supports two operational mode that are; (1) Mono E and RI modes and two coordinate input options, namely (1) text and (2) graphical modes. The GUI was developed using C++ programming language using the QT5 libraries (<https://www.qt.io/>). The graphical coordinate input was developed in C++ programming language using OpenGL application programming interface (<https://www.opengl.org/>). The dynamic phantom generator was written in the FORTRAN90 programming language and lastly the script/code viewer and collision detection modules

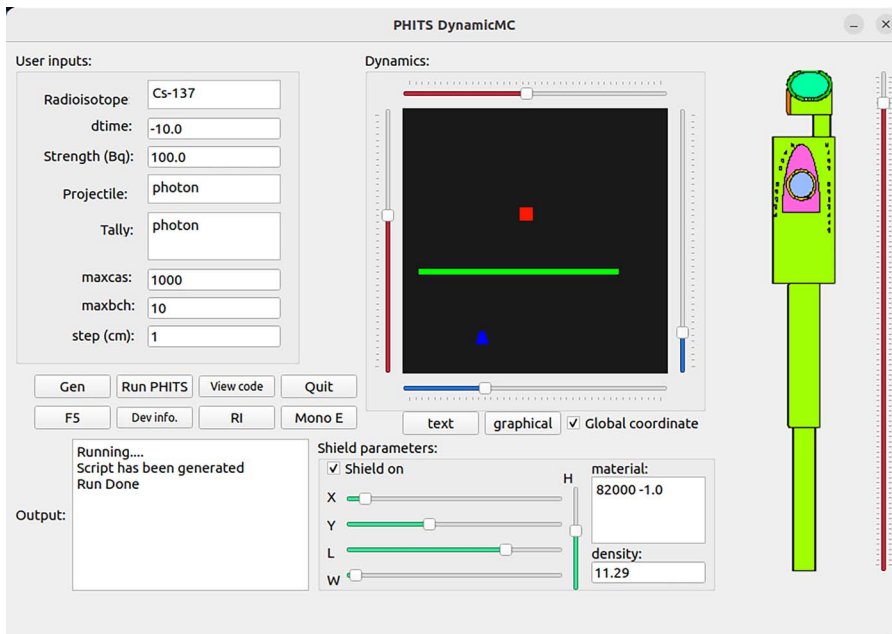


Figure 1. GUI of the PHITS DynamicMC platform showing the irradiation of human phantom with ^{137}Cs radioactive source with enabled shielding option.

were written in C++ programming language. Detailed description of these parts is given in the following sub-sections.

Graphical user interface

The GUI for the new version of DynamicMC has been designed to be more intuitive without having any complex functions. A snapshot of the program interface is shown in Fig. 1. The users can set the type of the radioisotope or incident particle, beam energy, tallies, maxcas, maxbch, step value (used to define increments in the dynamics movements) and five different sliders to manipulate the x and y positions of human phantom and the radioactive source, and the source z position with respect to the height of the modeled human phantom. In the text-based entry option, the users can numerically define the position of radioactive source (s_x , s_y , s_z) and human phantom (p_x , p_y). In addition, the shield option provides the users with the possibility of modeling a rectangular parallelepiped shield with user defined materials and density. The users have the ability to manipulate the x , y and z positions and also the length and width of the modeled shield using X, Y, H, L and W sliders, respectively. The black color window under *Dynamics* shown in Fig. 1 is the interactive graphical coordinate input based on the OpenGL. The red and blue markers represent the radioactive source and human phantom, respectively. The green rectangle represents the

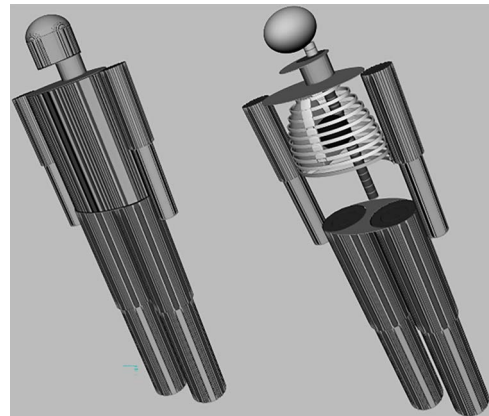


Figure 2. Three-dimensional snapshots of the implemented anthropomorphic phantom in the present platform.

modeled shielding between the radioactive source (i.e. red square) and the human phantom (i.e. blue marker). Considering the size of the implemented OpenGL window, markers that are small enough to fit within this window were chosen. It needs to be noted that the OpenGL window shows the relative position of the radioactive source and human phantom and provides an approximate position between these entities. However, we recommend PHIG3D viewer that comes in bundle with PHITS MC package for a more realistic three-dimensional view of the phantom (see Fig. 2).

Dynamic coordinate input

Considering the graphical coordinate input, unlike the previous version of the DynamicMC that used SFML (<https://www.sfml-dev.org/>) libraries with an external interactive window, the present version has an embedded graphical coordinate input module into the GUI (shown as a black window in Fig. 1). The x and y coordinates of the radioactive source and the human phantom can be manipulated using the horizontal and vertical sliders, respectively, that were placed around the interactive OpenGL window. The top and left sliders alter the x and y coordinates of the radioactive source by increment defined in the step variable in the GUI. The bottom and right sliders alter the x and y coordinates of the human phantom by increment defined in the step variable in the GUI. After moving the sliders to set the positions, users must click onto the interactive OpenGL window (i.e. the black color window) to update the positions of the radioactive source and the human phantom. The shielding option can be enabled using the *Shield on* checkbox and the shielding position and its dimensions can be manipulated using each slider shown in the shield parameters section. As mentioned in the previous sub-section, the red and blue squares represent the radioactive source and human phantom, respectively. The green rectangle represents the modeled shielding between the radioactive source and the human phantom. Lastly, the vertical slider next to the image of the modeled phantom sets the z position of the source with respect to the height of the human phantom.

Considering the text-based coordinate input, it can be enabled by clicking the *text* button as shown in Fig. 1. The location of the radioactive source and the human phantom can be numerically set for every position to score the required dosimetric quantities. The text-based coordinate input option would be useful for modeling large number of radioactive source and human phantom positions. The program will automatically loop over the user inputted data and perform the computations according to the parameters set by the user. It needs to be noted that the text-based option solely relies on the input from the users and therefore inputted radioactive source and human phantom positions must be without any geometrical overlaps.

As the first version of the program, we only considered a single radioactive source to simplify the task of absorbed dose approximation. Furthermore, the dynamic nature of the present program would further complicate the task of dosimetry when multiple radioactive sources are considered. In the future version of the present platform and computer program, we aim to further extend it to multiple radioactive source definitions.

```

[Title]
generated by PHITS DynamicMC

[Parameters]
icntl = 0
maxcas = 1000
maxbch = 10
ireschk = 1 # (D=0) Restart, 0:Check consistency, 1:No check
ih2o = 69
file(6) = phits.out

[Source]
s-type = 9
proj = photon
dir = all
r1 = 1.0E-10
r2 = 1.0E-10
x0 = 93.000
y0 = 120.000
z0 = 70.00
e-type = 28
  
```

Figure 3. Simple script/code viewer showing a generated script by PHITS DynamicMC.

Dynamic phantom generator

The model behind the dynamic phantom generator takes the user inputs from the GUI and the graphical coordinate input and builds the anthropomorphic phantom. We have adopted and modified the Medical Internal Radiation Dose Committee (MIRD) type anthropomorphic phantom that was previously developed⁽²³⁾ and also used⁽²⁴⁾. Some of the main considered organs in the present human phantom are the brain, skull, heart, left and right lung, rib cage, spine and vertebrae, head and neck, hands and legs, skeleton and skin. Upon phantom movement, the program automatically performs transformations in the xy plane, according to the user inputs, this transformation would take place globally over all organs that are present in the modeled phantom. However, for simplicity, the leg and hand movements during this vector transformation were not considered and therefore this dynamic movement resembles the upright standing position of a human in the radiation field. The three-dimensional snapshots of the employed human phantom are shown in Fig. 2.

Simple script/code viewer

The script/code viewer can be invoked by clicking onto the View code button embedded within the GUI (see Fig. 1) only after a successful run which in turn generates a PHITS script for a specific user-defined setup. The main reason for implementing this simple script/code viewer was to provide the option to users to swiftly inspect their script elements (that are rather lengthy) without requiring a third-party code/text editor. It needs to be noted that due to simplicity of the present script/code viewer, no specific syntax

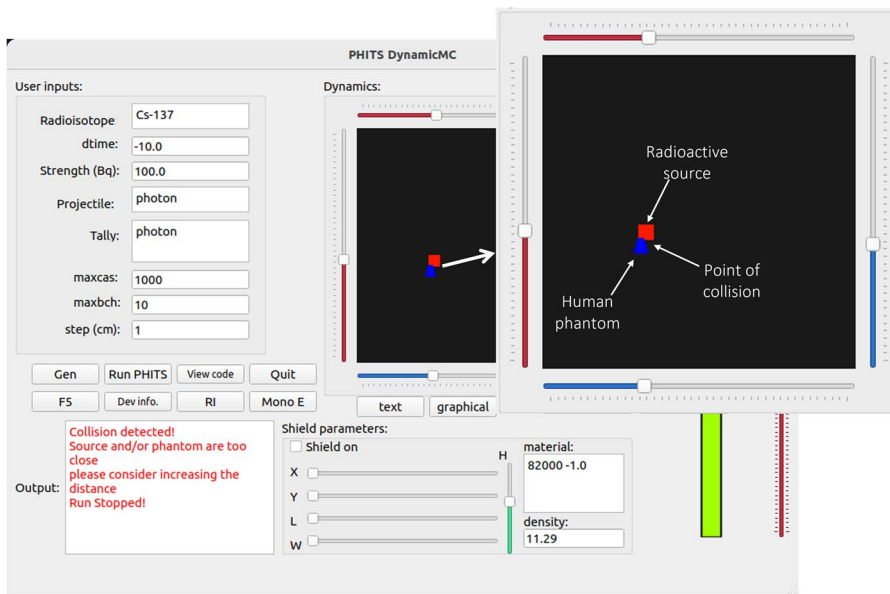


Figure 4. An example of collision detection between the modeled radioactive source and the modeled human phantom.

highlighting for PHITS MC package was implemented. We refer interested readers to our previous work⁽²⁵⁾ in which a terminal-based code editor with specific syntax highlighting was developed for PHITS MC package as part of the project. A snapshot of the developed script/code editor is shown in Fig. 3.

Simple collision detection module

In the initial version of DynamicMC⁽⁸⁾, the graphical coordinate input reported cases that were out of bound, which referred to the scenario where the radioactive source overlapped with the modeled human phantom. Since the present study focus on the exposure of human body to external radiation sources, the source was not defined to be in any of the modeled organs. In case of any overlaps, the generated script would be incorrect and cannot be executed using MC packages that were coupled with DynamicMC. For the enabled shield option, there should not be any overlap between the modeled shield and radioactive source and/or human phantom. To avoid such issues with the generated script, a simple collision detection module which is simply a function has been developed; this checks the x and y coordinates of the radioactive source with those of the modeled human phantom (and the shielding material in case of enabled shield option), and terminates the generation of the script if it detects any overlaps; this would be particularly useful to prevent users to end up with a wrong input script and in turn saves debugging time and effort. The outer boundaries of the modeled human phantom are used to set a hard cutoff value to accomplish this task. An example of collision detection

for disabled shield option is shown in Fig. 4 where the red square (i.e. radioactive source) and blue marker (i.e. human phantom) are in a close proximity and therefore the program presents an output error message in its dialog box.

Radiation transport parameters and tallies

The present version of DynamicMC models a spherical source with radius of 1.0×10^{-10} cm that emits primary radiation in all directions; this is similar to an isotropic point source which we have considered previously^(4,8). Considering the RI mode, the type of radioisotope can be defined as Cs-137, Co-60, etc. In addition, the time evolution (dtim), source strength, projectile emitting from the radioisotope source. Considering the Mono E mode, total of four different incident particles can be chosen from the dropdown menu in the GUI that are protons, neutrons, photons and alpha particles. Since the present platform focuses on the point source model, the use of X-ray tube would be out of its scope, given that X-ray tube used in medical physics/imaging are those collimated beams with specific energy spectra. The present platform was built for radiation protection studies where a point source emits radiation dynamically in all directions (i.e. isotropic). It is possible to emulate an X-ray tube using DynamicMC by placing point sources along the orbit of the X-ray tube. However, this requires continual and specific energy spectrum implementation which is highly case dependent. Presently, the web system named WAZA-ARI⁽²⁶⁾ calculates X-ray distribution for many manufacturers using PHITS. In future versions of the present platform

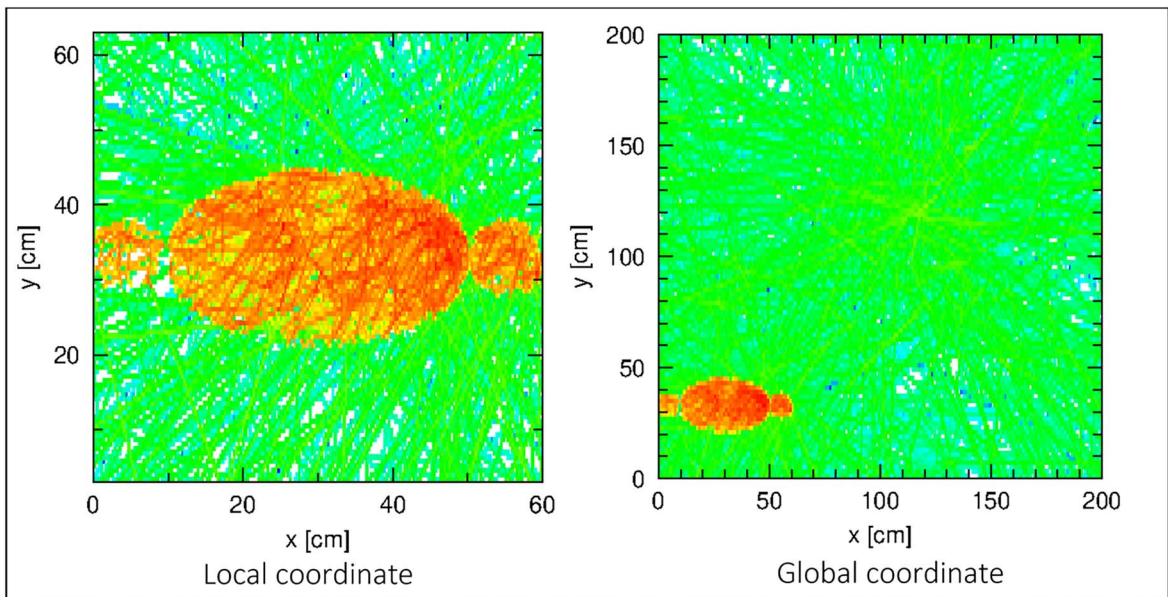


Figure 5. Difference between the local and global coordinate definition for geometrical boundaries of autogenerated tallies in the present model. The color intensity represents the energy deposition.

and computer program, we aim to further extend it for medical physics/imaging related beams and therefore will consider continuous energy spectra from those X-ray tubes with appropriate collimation and energy spectrum using WAZA-ARI and PHITS MC package. The material compositions for the modeled human phantom are fixed for both modes and the surrounding ambient material is assumed to be dry air at sea level. The material compositions and densities can be checked in the generated scripts.

The ICRP Publication 103⁽²⁷⁾ considered 15 major organs including red bone marrow (RBM), colon, lungs, stomach, gonads, bladder, esophagus, liver, thyroid, endosteum (bone surface), brain, salivary glands, skin, and remainder tissues; this is particularly useful for organs that are considered in most radiation dosimetry studies⁽²⁸⁾. A total of three main different tallies will be generated for every user-defined case, namely (1) T-Gshow, (2) T-Deposit that generate two-dimensional geometrical view and dose deposition plots and (3) T-Deposit dose deposition in six selected organs. These selected organs are as follows: (1) left lung, (2), right lung, (3) heat tissue and blood, (4) spine and discs, (5) brain and (6) head and face skin.

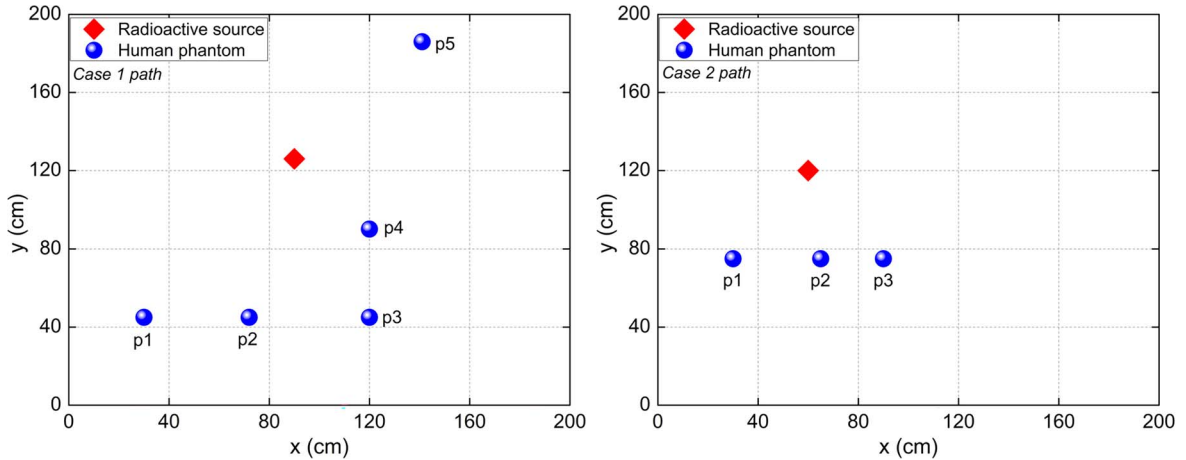
Considering the two-dimensional energy deposition tallies, three different planes of view would be considered for both T-Gshow and T-Deposit tallies, namely (1) xz , (2) xy , (3) yz that with their output names bearing the (1) front, (2) top and (3) side view tags, respectively. Lastly, for every tallied particle in the

modeled system, each of the three different planes of views will be generated; this makes visualisation of dose dispersion and radiation transport much more convenient for interested users. It is worth noting that considering all possible tallies would not be feasible as it is dependent on the user's choice. However, the present version of DynamicMC coupled with PHITS MC package provides much higher flexibility when compared to the previous version that was coupled with MCNP MC package; this is mainly due to the features that are exclusively provided by PHITS MC package that enabled the implementation of multiple features such as definition of user-defined radioisotope source with energy spectrum beam and automatic averaging of organ doses along the path of the phantom using RI-source and sumtally functions of PHITS MC package, respectively.

The geometrical bound for the generated tallies can be defined in two ways either in local or global coordinate manner; it is important to note that this option only works for the two-dimensional energy deposition cases, mainly due to the fact that a spatial energy deposition could only be observed using this tally option. The term local refers to the tally boundaries that embrace the body of the human phantom; this does not present a larger view of the modeled setup and can be useful if one wishes to study radiation transport inside the modeled human phantom. The term global refers to the tally boundaries that embrace the entire modeled system defined by the

Table 1. Parameters used in two different case studies using the developed platform.

Case	Particle	Energy	Tallies	Step (cm)	No. positions
Case 1	Photon	^{137}Cs energy spectrum	Photon	1	5
Case 2	Neutron	5.0 MeV	Neutron	1	3

**Figure 6.** Chosen human phantom paths for cases 1 and 2 as viewed from the xy plane.

size of the step value; this presents a larger view of the modeled setup in which the radioactive source, human phantom model and ambient air can be seen. The users can switch the global coordinate definition on or off by checking or unchecking the checkbox in the GUI (see Fig. 1), respectively. In case of unchecked global coordinate definition, the model defaults to local coordinate boundaries. In order to demonstrate this feature, an example run with local and global coordinate definition is shown in Fig. 5.

Considering the multi-particle feature of the present program that supports proton, neutron, photon and alpha particles and those radioisotopes that emit these projectiles, different physics and models will be used to determine the dose deposition. Considering charged particles, the Intra-Nuclear Cascade Liege (INCL) model was used to explain the nuclear reaction involved in the present work. The INCL was implemented as the default model for simulating nuclear reactions induced by protons. The stopping powers for charged particles and nuclei were calculated using the ATIMA code <https://web-docs.gsi.de/~weick/atima/>. Considering uncharged particles, the Kerma approximation was used to determine the energy deposition by employing T-Deposit tally function provided by the PHITS MC package. We refer interested readers to Ref.⁽²⁹⁾ and references therein for more information regarding the employed physical models for calculation of dose deposition.

Computational scheme

There are a large number of possible setups that can be modeled using the present platform and it would not be feasible to consider all possibilities. For information regarding all the features that the new version of DynamicMC offers after coupling with PHITS MC package, we refer the readers to the user manual that can be found from: https://figshare.com/articles/software/Development_of_DynamicMC_for_PHITS_Monte_Carlo_package/22731920. Therefore, to demonstrate the capabilities of the present program, two examples were chosen. A total of two cases with different incident particles, energies, tallies, step values and number of dynamic positions without the presence of any shielding material were considered; these are listed in Table 1.

The chosen paths for cases 1 and 2 that the human phantom will undertake are shown in Fig. 5. The paths are viewed from the xy plane (*i.e.*, top view) that shows the relative movement of phantom with respect to the radioactive source. In addition, for both cases, the height position (along the z -axis) has been assumed to be fixed at 70 cm. Using the generated paths shown in Fig. 6, the dose dispersion snapshots from different points of view (top, front and side view) were scored. In addition, the photon dose deposited in the selected organs were also determined for both cases.

Lastly, the effect of 1 and 10 cm lead shielding against ^{137}Cs photons for the modeled human phantom was

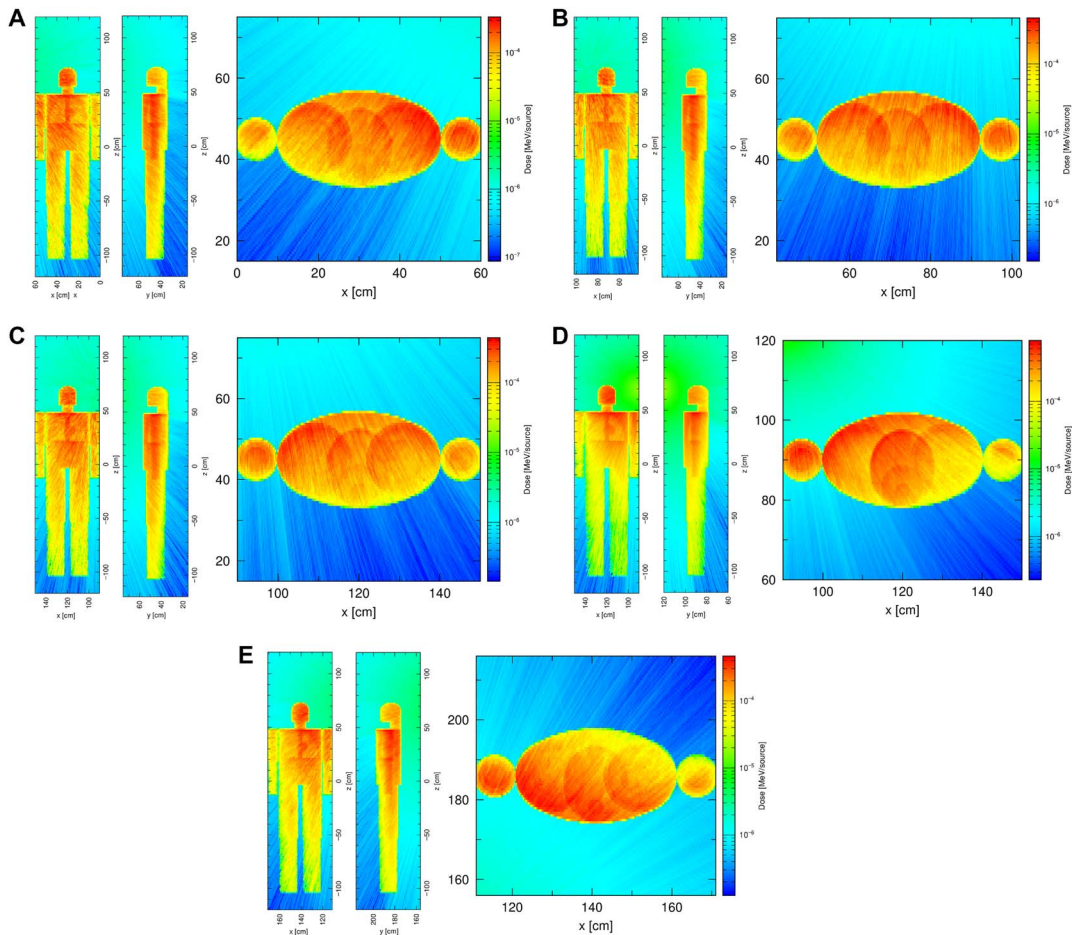


Figure 7. Two-dimensional energy deposition snapshots from photon emitted from the ^{137}Cs radioisotope obtained from the front (left), top (center) and side (right) views for (a) $p1$, (b) $p2$, (c) $p3$, (d) $p4$ and (e) $p5$ human phantom positions in a radiation field. In the present case, the source refers to incident photons.

considered. The radioactive source was fixed at (60, 102, 40) cm position, emitting ^{137}Cs photons isotropically and the human phantom kept fixed at the (45, 30) cm position. The shielding material was placed between the radioactive source and the human phantom. The dosimetric results before and after shielding were scored in the selected organs. In addition, the two-dimensional energy deposition snapshots from different views were also prepared.

For both example cases, a total of 10^6 incident particles were assumed to be emitted from an isotropic spherical radioactive source with a radius of 10^{-10} cm, which resembled a point source. The dose deposition in the selected organs were scored in the unit of Gy/initial particles and Gy/s for Mono E and RI mode, respectively. The two-dimensional energy depositions were scored in the unit of MeV/initial particles. All data, source codes, executable programs (for both

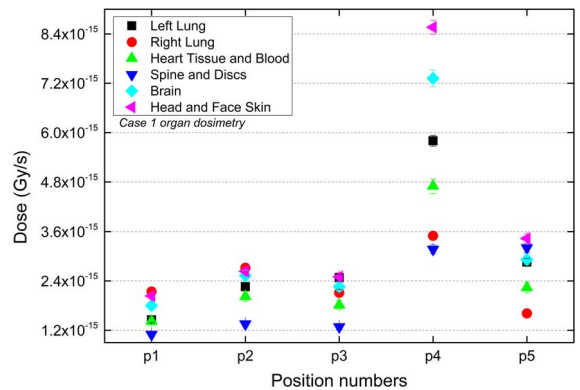


Figure 8. Dose deposition in six selected organs upon exposure to photons emitted from ^{137}Cs radioisotope at position $p1$, $p2$, $p3$, $p4$ and $p5$. All values were obtained with less than $\sim 6\%$ of average relative error.

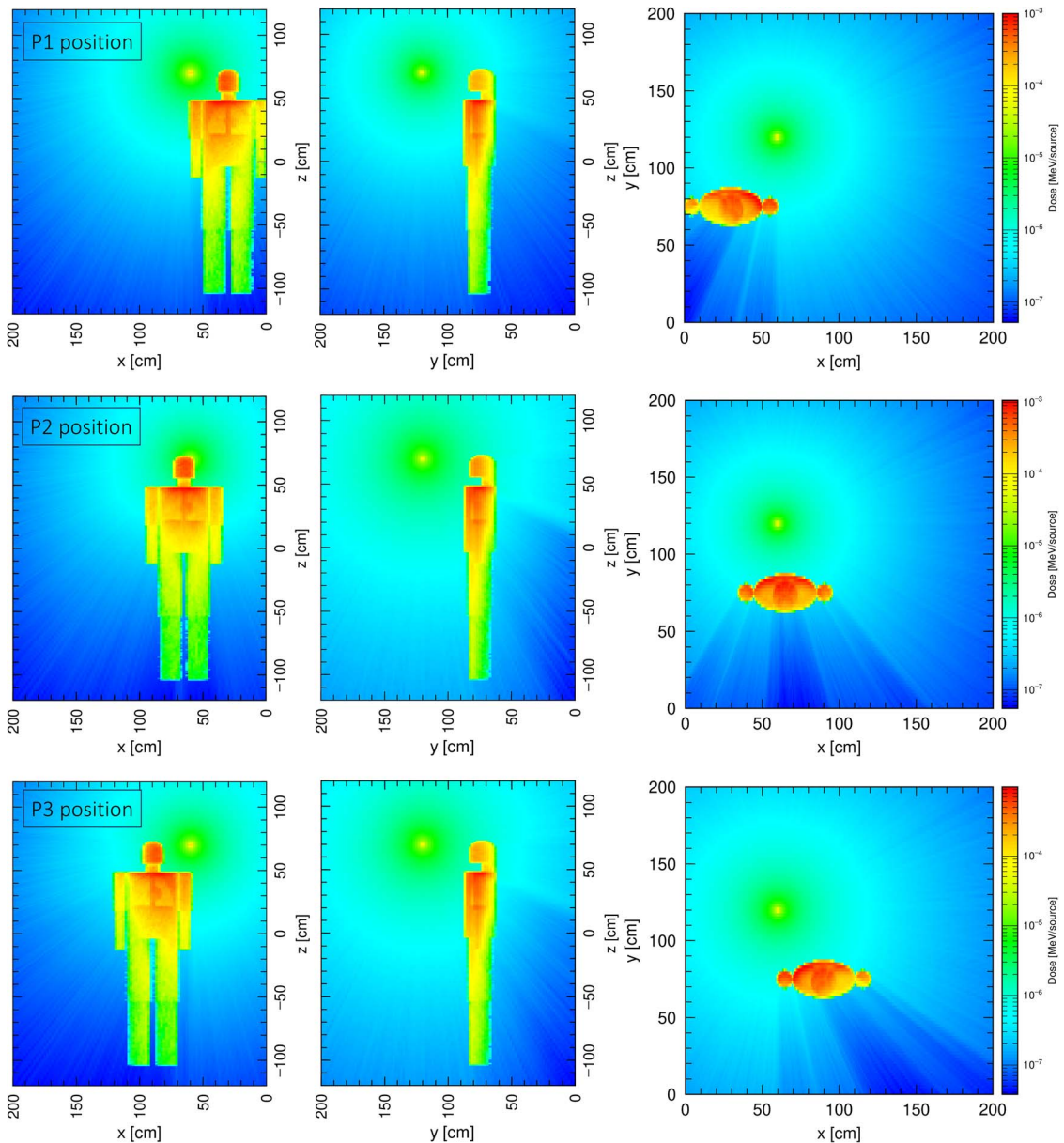


Figure 9. Two-dimensional energy deposition snapshots from 5 MeV neutrons obtained from the front (left), top (center) and side (right) views for (a) $p1$, (b) $p2$ and (c) $p3$ human phantom positions in a radiation field. In the present case, the source refers to incident neutrons.

GNU/Linux and Microsoft Windows operating systems) including the example input and output files that were shown in Table 1 can be downloaded from https://figshare.com/articles/software/Development_of_DynamicMC_for_PHITS_Monte_Carlo_package/22731920

Results and discussion

The results of two-dimensional energy deposition for five different human phantom positions for case 1 are shown in Fig. 7(a–e). In case 1, the local coordinate option that was discussed in Section 2.2 was used to only view the human phantom domain in the radiation

field. For each position, three points of view were considered, namely the (1) front, (2) top and (3) side views. From the results shown in Fig. 7(a–e), the energy deposition from photons tend to reduce with increasing distance between the radioactive source and human phantom. Furthermore, the orientation of the human phantom with respect to the radioactive source can significantly alter the energy deposition in different organs. The results shown in Fig. 7 show that the relative position between the radioactive source and human phantom is an important parameter, given that the energy deposition can vary in different parts of the human body as it moves in an isotropic radiation field; this can be observed from the dose deposited in six different selected organs as shown in Fig. 8. The path that was chosen for the case 1 is shown in Fig. 6 and the closest relative position between the radioactive source and the human phantom is at position $p4$. Subsequently, from the dose results shown in Fig. 8, the highest dose in selected organs were scored at position $p4$.

The multi-tally capability offered by the current version of DynamicMC makes the task much easier for users to score energy/dose deposition from primary and secondary radiations in their modeled system. We believe this will be important for clinical applications where incident radiation energies are increasing to a level at which generation and dose contribution from primary and secondary radiation are becoming significant⁽³⁰⁾⁽³¹⁾.

Considering case 2 (see Table 1), a total of three positions were used to score the energy deposition by neutrons. The global coordinate option that was discussed in Section 2.2 was used to only view a larger picture of the human phantom irradiation in the radiation field. For simplicity, no secondary radiations were scored for this example. Similar to case 1, for each position, three points of view were considered, namely the (1) top, (2) front and (3) side views obtained from the xy , xz and yz planes, respectively. The results for energy deposition from these three point of views are shown in Fig. 9. As discussed in case 1 above, energy deposition in the body of the human phantom tended to decrease with increasing distance from the source; this can be explained by the reduction of particle fluence and attenuation in ambient air as a result of increasing relative distance between the radioactive source and the human phantom. The deposited dose in the six selected organs for position $p1$ to $p3$ are shown in Fig. 10.

The highest dose deposition in the selected organs from 5 MeV neutrons found to be for the $p2$ position. Considering the path for case 2, as shown in Fig. 6, the position $p2$ has the shortest distance between radioactive source and the human phantom; this, in turn, leads to a higher dose deposition in the selected organs as

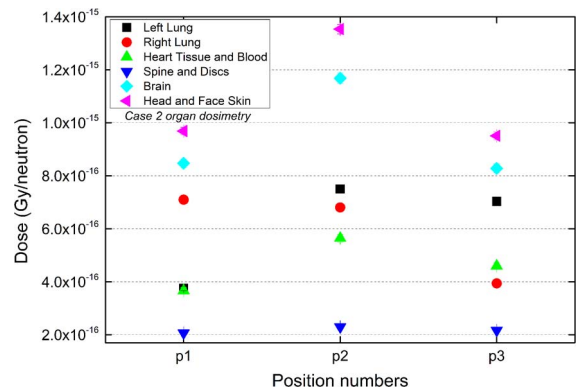


Figure 10. Dose deposition in six selected organs upon exposure to 5 MeV neutrons at position $p1$, $p2$ and $p3$. All values were obtained with less than $\sim 6\%$ of average relative error.

shown in Fig. 10 for position $p2$. The orientation of the human phantom with respect to the radioactive source has the ability to alter the dose in different organs. From the results shown in Fig. 10, the dose deposited in right lung found to be higher for $p1$ case when compared to $p3$; this is due to the orientation of the phantom that faces the positive y -axis. In case of $p1$ position, the right lung is closer to the radioactive source when compared to the $p3$ position and therefore the variation in the dose deposition can be clearly observed as the human phantom moves along the positive x -axis. Another interesting observation would be the energy deposition in the ambient air after interacting with the body of the human phantom; this can be clearly seen from the top view for $p1$, $p2$ and $p3$ shown in Fig. 9. The energy deposition from 5 MeV neutrons tends to be lower after propagating through the body of human phantom, mainly due to subsequent energy loss and attenuation. This subsequent energy loss can only be viewed when the global coordinate option is enabled, which demonstrates another useful feature of the current version of DynamicMC platform.

Lastly, the effect of 1 and 10 cm lead shielding has been investigated for the emitted photons from ^{137}Cs radioisotope. The shielding option (see Fig. 1) provided in the current version of DynamicMC has been used to demonstrate the capabilities of the present platform. The two-dimensional energy deposition from incident photons observed from side view for cases without and with shielding are shown in Fig. 11. From Fig. 11, it can be seen that applying the 1 and 10 cm lead shield reduces energy deposition in the modeled human body and its organs⁽⁴⁾. The results in Fig. 11 demonstrate the capability of the present program to successfully model shielding and its effects on the energy deposition. In addition to the two-dimensional energy deposition snapshots, the dose in the six selected organs were

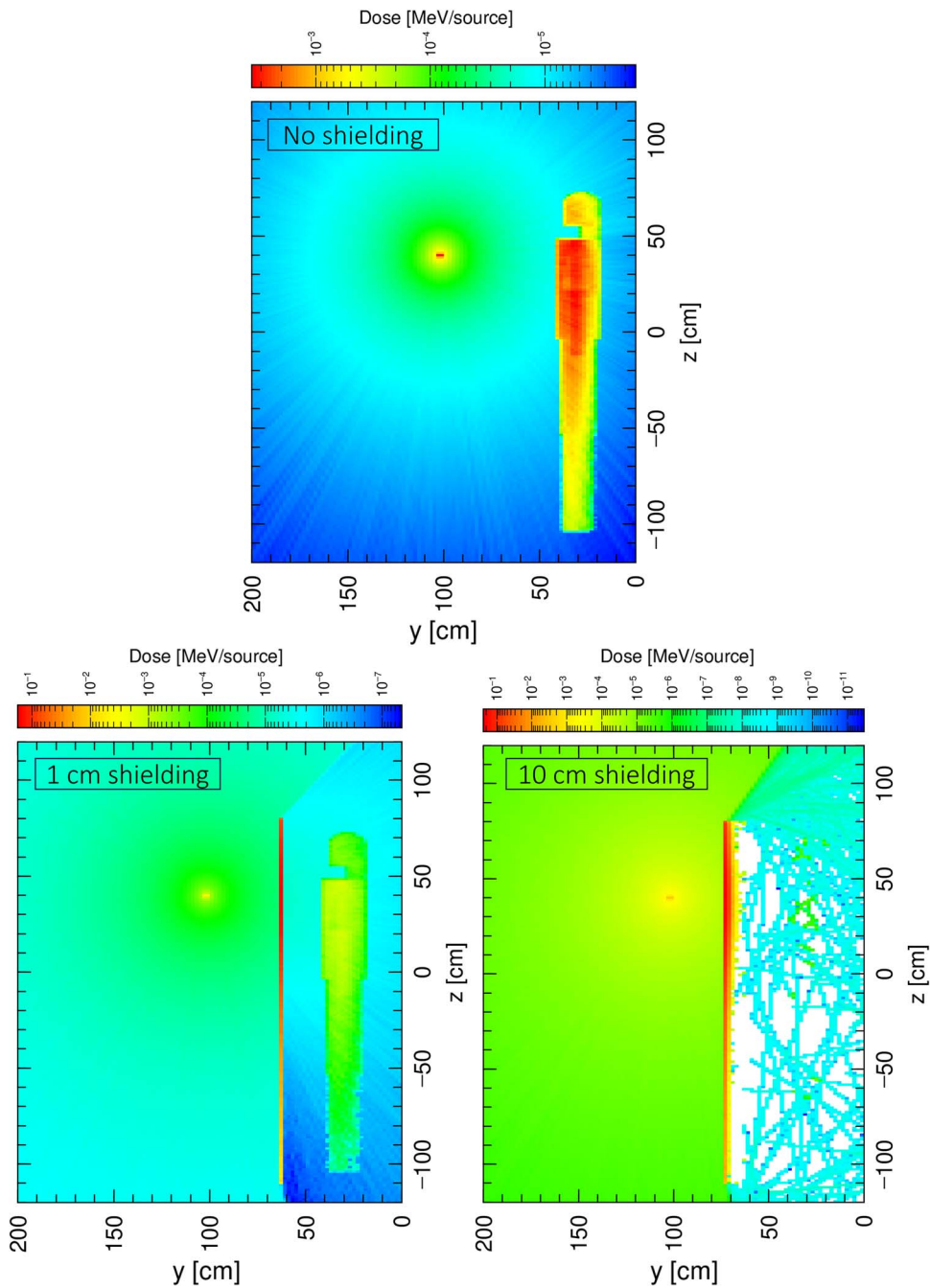


Figure 11. Two-dimensional side view energy deposition snapshots from the photons emitted by ^{137}Cs radioisotope for the case without and with 1 and 10 cm lead shielding. In the present case, the source refers to incident photons.

determined for the cases without and with 1 and 10 cm shielding and shown in Fig. 12. Considering the results shown in Fig. 12, L.Lung, R.Lung, Heart&, Spine& and Head& correspond to left lung, right lung, heart tissue and blood, spine and discs and head and face skin, respectively.

Applying lead shielding between the radioactive source and the human phantom, the deposited photon dose in the six selected organs reduces. Furthermore, the higher thickness of the lead shielding materials tends to be more effective in reducing the photon dose deposited in the selected organs. In our previous

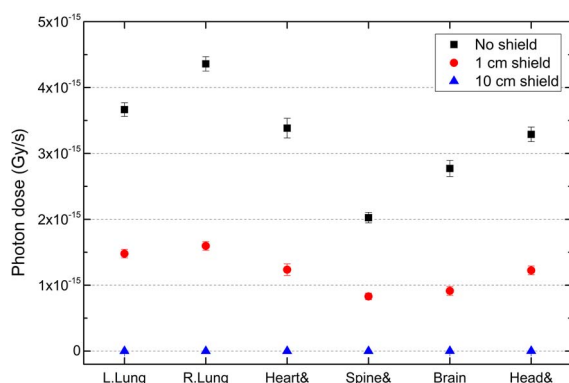


Figure 12. Dose deposition in six selected organs upon exposure to photons emitted by ^{137}Cs radioisotope for the case without and with 1 and 10 cm lead shielding. All values were obtained with less than $\sim 6\%$ of average relative error.

work⁽⁴⁾, we have observed similar trends when applying lead shielding to the ORNL human phantom exposed to photons emitted from ^{137}Cs radioisotope. Considering the obtained results, the presence of the shielding option would be useful for studying dose reduction for different shielding materials. The present feature would also be important to investigate the effect of dynamic movement of radioactive source and/or human phantom in presence of shielding materials in occupational environments.

Summary and conclusions

In the present work, an open-source and easy-to-use platform named PHITS DynamicMC has been developed for modeling the irradiation of an anthropomorphic phantom with and without shielding materials. The present version of the platform has been coupled with the PHITS MC package and allows users to move the radioactive source and the modeled human phantom in the three-dimensional Cartesian coordinate system; this will be particularly useful when studying radiation dosimetry for occupational workers. Users have the ability to study radioisotopes with precise decay scheme and energy spectrum and four different Mono E incident ionising radiations, namely (1) protons, (2) neutrons, (3) photons and (4) alpha particles. The modeling definition of organs in the human phantom, MC parameters and source definition and tallies will be set automatically by the program. Furthermore, users have the ability to model different shielding materials and investigate its impact on energy deposition in the human phantom and the surrounding environment. The current version of DynamicMC provides a higher flexibility for dynamic movement for an anthropomorphic phantom; this tends to reduce the computational cost and complexity. The newly added features utilise

those functions that are only provided by the PHITS MC package, which presents novel additions to the previous MCNP-based version of the program. This program natively supports multiple widely used operating systems and we expect that the present work and the developed tools would be useful for researchers in the field of nuclear radiation physics.

Data availability

All data, executables and source code files and program manual can be downloaded from https://figshare.com/articles/software/Development_of_DynamicMC_for_PHITS_Monte_Carlo_package/22731920.

Funding

The present work was supported by the Japan Society for the Promotion of Science KAKENHI grant numbers 20H03615, 21F21103, JPJSBP120218804, 23H03774 and 23K07087, as well as CityU grant numbers 9220124 and 9229151 and by the Ministry of Science, Technological development and Innovation of the Republic of Serbia No 451-03-47/2023-01/200122.

Conflict of interest

The authors declare that there are no conflicts of interest.

References

- Ryan, J. L. *Ionizing radiation: the good, the bad, and the ugly*. *J. Invest. Dermatol.* **132**, 985–993 (2012).
- Desouky, O., Ding, N. and Zhou, G. *Targeted and non-targeted effects of ionizing radiation*. *J. Radiat. Res. Appl. Sci.* **8**, 247–254 (2015).
- Cerutti, P. A. *Effects of ionizing radiation on mammalian cells*. *Sci. Nat.* **61**, 51–59 (1974).
- Shahmohammadi Beni, M., Watabe, H., Krstic, D., Nikezic, D. and Yu, K. N. *MCHP (Monte Carlo+ human phantom): platform to facilitate teaching nuclear radiation physics*. *PLoS One* **16**, e0257638 (2021).
- Shahmohammadi Beni, M., Krstic, D., Nikezic, D. and Yu, K. N. *Monte Carlo studies on photon interactions in radiobiological experiments*. *PLoS One* **13**, e0193575 (2018).
- Aghaz, A., Kardan, M. R., Deevband, M. R., Bahadorzadeh, B., Kasesaz, Y. and Ghadiri, H. *Patient-specific dose assessment using CBCT images and Monte Carlo calculations*. *J. Instrum.* **16**, P10011 (2021).
- Kim, J. H. *Three principles for radiation safety: time, distance, and shielding*. *Korean J. Pain* **31**, 145–146 (2018).
- Yu, K. N. *et al.* *DynamicMC: an open-source GUI program coupled with MCNP for modeling relative dynamic movement of radioactive source and ORNL phantom in a 3-dimensional radiation field*. *Health Phys.* **124**, 301–309 (2023).
- X-5 Monte Carlo Team. *MCNP—A General Monte Carlo N-particle Transport Code, Version 5* (Los Alamos, NM:

- Los Alamos National Laboratory) p. LA-UR-03-1987 (2003).
10. Akkurt, H., Eckerman, K. F., Wagner, J. C. and Sherbini, S. *PIMAL: computational phantom with moving arms and legs*. *Trans. Am. Nucl. Soc.* **96**, 396 (2007).
 11. Hiller, M. M., Bellamy, M. B., Akkurt, H., Wiarda, D., Kora, G. H., Eckerman, K. F., Griffin, K., Oxenberg, T., Sherbini, S. and Saba, M. *PIMAL: Phantom with Moving Arms and Legs Version 4.1.0* (Oak Ridge, TN: Oak Ridge National Lab. (ORNL)) (2017).
 12. Auvinen, A., Pukkala, E., Hyvönen, H., Hakama, M. and Rytömaa, T. *Cancer incidence among Finnish nuclear reactor workers*. *J. Occup. Environ. Med.* **1**, 634–638 (2002).
 13. Boice, J. Jr., Dauer, L. T., Kase, K. R., Mettler, F. A. Jr. and Vetter, R. J. *Evolution of radiation protection for medical workers*. *Br. J. Radiol.* **93**, 20200282 (2020).
 14. Ewing, R. C., Weber, W. J. and Clinard, F. W. Jr. *Radiation effects in nuclear waste forms for high-level radioactive waste*. *Prog. Nucl. Energy* **29**, 63–127 (1995).
 15. Weber, W. J. and Roberts, F. P. *A review of radiation effects in solid nuclear waste forms*. *Nucl. Technol.* **60**, 178–198 (1983).
 16. Demir, M., Demir, B., Sayman, H., Sager, S., Sabbir Ahmed, A. and Uslu, I. *Radiation protection for accompanying person and radiation workers in PET/CT*. *Radiat. Protect. Dosim.* **147**, 528–532 (2011).
 17. Olko, P., Currivan, L., Van Dijk, J. W., Lopez, M. A. and Wernli, C. *Thermoluminescent detectors applied in individual monitoring of radiation workers in Europe—a review based on the EURADOS questionnaire*. *Radiat. Protect. Dosim.* **120**, 298–302 (2006).
 18. Sneha, C., Pradhan, S. M. and Adtani, M. M. *Study of minimum detection limit of TLD personnel monitoring system in India*. *Radiat. Protect. Dosim.* **141**, 168–172 (2010).
 19. Hsu, S. M., Yeh, S. H., Lin, M. S. and Chen, W. L. *Comparison on characteristics of radiophotoluminescent glass dosimeters and thermoluminescent dosimeters*. *Radiat. Protect. Dosim.* **119**, 327–331 (2006).
 20. Shahmohammadi Beni, M., Krstic, D., Nikezic, D. and Yu, K. N. *A comparative study on dispersed doses during photon and proton radiation therapy in pediatric applications*. *PLoS One* **16**, e0248300 (2021).
 21. Shahmohammadi Beni, M., Ng, C. Y., Krstic, D., Nikezic, D. and Yu, K. N. *Conversion coefficients for determination of dispersed photon dose during radiotherapy: NRURad input code for MCNP*. *PLoS One* **12**, e0174836 (2017).
 22. Endo, A., Yamaguchi, Y. and Eckerman, K. F. *Nuclear decay data for dosimetry calculation - revised data of ICRP Publication 38*. *J. Agric. Ecol. Res. I* **1347** (2005).
 23. Lee, D. *Simulation and Analysis of Human Phantoms Exposed to Heavy Charged Particle Irradiations Using the Particle and Heavy Ion Transport System (PHITS)*. Doctoral dissertation (Texas A & M University) (2012).
 24. Islam, M. R. *et al.* *A feasibility study on proton range monitoring using ¹³N peak in inhomogeneous targets*. *Tomography* **8**, 2313–2329 (2022).
 25. Shahmohammadi Beni, M., Islam, M. R., Kim, K. M., Krstic, D., Nikezic, D., Yu, K. N. and Watabe, H. *On the effectiveness of proton boron fusion therapy (PBFT) at cellular level*. *Sci. Rep.* **12**, 18098 (2022).
 26. Takahashi, E., Sato, K., Endo, A., Ono, K., Yoshitake, T., Hasegawa, T., Katsunuma, Y., Ban, N. and Kai, M. *WAZA-ARI: computational dosimetry system for X-ray CT examinations. I. Radiation transport calculation for organ and tissue doses evaluation using JM phantom*. *Radiat. Protect. Dosim.* **146**, 241–243 (2011).
 27. International Commission on Radiological Protection. *The 2007 Recommendations of the International Commission on Radiological Protection*. ICRP Publication 103. *Ann. ICRP* **37** (2–4) (Elsevier) (2007).
 28. Zivkovic, M., Shahmohammadi Beni, M., Yu, K. N., Watabe, H., Krstic, D. and Nikezic, D. *A dosimetric comparison between ICRP and ORNL phantoms from exposure to ¹³⁷Cs contaminated soil*. *Radiat. Phys. Chem.* **207**, 110878 (2023).
 29. Sato, T. *et al.* *Features of Particle and Heavy Ion Transport Code System (PHITS) version 3.02*. *J. Nucl. Sci. Technol.* **55**, 684–690 (2018).
 30. Janiszewska, M., Karaczyn, B., Grelik, K. P. and Konefa, A. *Secondary radiation dose during high-energy TBI*. *Int. J. Radiat. Oncol. Biol. Phys.* **78**, S637 (2010).
 31. Banaee, N., Goodarzi, K. and Nedaie, H. A. *Neutron contamination in radiotherapy processes: a review study*. *J. Radiat. Res.* **62**, 947–954 (2021).